Structural Engineering and Mechanics, Vol. 11, No. 2 (2001) 221-236
DOI: http://dx.doi.org/10.12989/sem.2001.11.2.221

A local point interpolation method for stress analysis of two-dimensional solids

G.R. Liu† and Y.T. Gu‡

Dept. of Mechanical Engineering, National University of Singapore,
10 Kent Ridge Crescent, Singapore 119260

Abstract. A local point interpolation method (LPIM) is presented for the stress analysis of two-dimensional solids. A local weak form is developed using the weighted residual method locally in two-dimensional solids. The polynomial interpolation, which is based only on a group of arbitrarily distributed nodes, is used to obtain shape functions. The LPIM equations are derived, based on the local weak form and point interpolation. Since the shape functions possess the Kronecker delta function property, the essential boundary condition can be implemented with ease as in the conventional finite element method (FEM). The presented LPIM method is a truly meshless method, as it does not need any element or mesh for both field interpolation and background integration. The implementation procedure is as simple as strong form formulation methods. The LPIM has been coded in FORTRAN. The validity and efficiency of the present LPIM formulation are demonstrated through example problems. It is found that the present LPIM is very easy to implement, and very robust for obtaining displacements and stresses of desired accuracy in solids.

Key words: meshless method; stress analysis; interpolation function; weak form; strong form.

1. Introduction

In recent years, a new class of numerical methods, namely, the element-free method or meshless method, has been developed. Meshless methods may be largely divided into two categories: domain-type methods and boundary-type methods. In these two types of meshless methods, the problem domain or only the boundary of the problem domain is discretized with properly scattered points. Several domain-type meshless methods, such as, the diffuse element method (Nayroles *et al*. 1992), element-free Galerkin (EFG) method (Belytschko *et al.* 1994), reproducing kernel particle method (Liu *et al.* 1995), point interpolation method (PIM) (Liu and Gu 1999), point assembly method (PAM) (Liu 1999), have been proposed and have achieved remarkable progress in solving a wide range of problems. The boundary-type meshless methods proposed include the boundary node method (BNM) (Kothnur *et al*. 1999) and boundary point interpolation method (BPIM) (Gu and Liu 2000a). In addition, techniques for coupling meshless methods with other established numerical methods have also been proposed, such as the coupled EFG/finite element method (FEM) (Belytschko and Organ 1995, and Hegen 1996), EFG/boundary element method (BEM) (Gu and Liu 2000b, and Liu and Gu 2000a), and EFG/BPIM (Liu and Gu 2000b).

† Professor
‡ Ph.D Candidate Student

The difference in these domain-type meshless methods comes mainly from the interpolation techniques used. In particular, the above-mentioned meshless methods are “meshless” only in terms of the interpolation of the field variables, as compared to the usual FEM. Most of meshless methods have to use background cells to integrate a weak form over the problem domain. The requirement of background cells for integration makes the method not “truly” meshless.

A domain-type truly meshless method, called the meshless local Petrov-Galerkin (MLPG) method, has been developed by Atluri and Zhu (1998, 2000), and Atluri *et al*. (1999). The MLPG method is based on a local weak form and a moving least squares (MLS) approximation. In the MLPG, an integration method in a regular-shaped local domain (such as spheres, rectangles, and ellipsoids) is used. There are two characteristics of the MLPG method. First, it is a truly meshless method in terms of not only non-element interpolation, but also non-mesh integration. Second, the implementation procedure is as simple as numerical methods based on the strong form formulation, such as the finite difference method (FDM).

However, there exist some inconveniences or disadvantages in using the MLPG. First, it is difficult to implement essential boundary conditions in the MLPG because the shape functions, constructed with the MLS approximation, lack the delta function property. Second, the MLPG is computationally expensive due to, again, the use of the MLS approximation. In addition, when the MLPG changes the integration domain from global to local, the problem related to local integrations becomes a new issue.

Some special techniques have to be used to overcome the above-mentioned problems in using the MLPG. For example, the Lagrange multiplier method, the penalty method (Atluri *et al*. 1999), the constraint MLS method (Liu *et al*. 2000), and the direct interpolation method (Liu and Yan 2000) have been used to deal with essential boundary conditions. The Lagrange multiplier method leads to an unbanded non-positive definite stiffness matrix, which increases significantly the difficulty in solving the discrete equations. The use of the penalty method requires a proper choice of the penalty factor, which can be difficult for some practical problems. The constraint MLS method is computationally very expensive. The direct interpolation method seems to be so far the simplest way to impose the essential boundary condition in the MLPG method.

A local point interpolation method (LPIM) is presented in this paper for two-dimensional solids, in which a set of points is used to represent the problem domain. A technique is proposed for constructing polynomial interpolation functions with the delta function property. A weak form is developed using the weighted residual method locally, based on the idea of MLPG (Atluri and Zhu 1998). The LPIM equations are then derived using the local weak form and the point interpolation approximation. The present LPIM is a truly meshless method, which performs interpolation without using elements and evaluates integrals without a background mesh. Moreover, since the shape functions possess the delta function property, the imposition of essential boundary conditions in LPIM is as easy as in the traditional FEM.

An LPIM program is coded in FORTRAN, and several numerical examples are presented to demonstrate the convergence, validity and efficiency of the LPIM.

2. Basic equations of elastostatics

Consider the following two-dimensional problem of solid mechanics in a domain Ω bounded by Γ:

$$\sigma_{ij,j}+b_i=0 \text{ in } \Omega \tag{1}$$

where σ_{ij} is the stress tensor, which corresponds to the displacement field u_i, b_i is the body force tensor, and $(\ )_{,i}$ denotes $(\partial/\partial x_i)$. The boundary conditions are given as follows:

$$\sigma_{ij}n_j=\bar{t}_i \text{ on the natural boundary } \Gamma_t \tag{2}$$

$$u_i=\bar{u}_i \text{ on the essential boundary } \Gamma_u \tag{3}$$

in which the $\bar{u}_i$ and $\bar{t}_i$ denote the prescribed displacements and tractions, respectively, and n_j is the unit outward normal to domain Ω.

3. Point interpolation approximation

In general, a meshless method requires a local interpolation or approximation to represent the trial function. The point interpolation approximation is used in the current work.

Consider a function $u(x)$ defined in domain Ω discretized by a set of field nodes. The point interpolates $u(x)$ from the surrounding nodes of a point x_Q using the polynomials

$$u(x, x_Q)=\sum_{i=1}^{n} p_i(x)a_i(x_Q)=\boldsymbol{p}^T(x)\boldsymbol{a}(x_Q) \tag{4}$$

where $p_i(x)$ is a monomial in the space coordinates $\boldsymbol{x}^T=[x, y]$, n is the number of nodes in the neighborhood of x_Q, $a_i(x_Q)$ is the coefficient for $p_i(x)$ corresponding to the given point x_Q. The $p_i(x)$ in Eq. (4) is built utilizing Pascal's triangle shown in Fig. 1, so that the basis is complete. A basis in one dimension is provided by

$$\boldsymbol{p}^T(x)=[1, x, x^2, x^3, x^4,\ldots] \tag{5}$$

A basis in two dimensions is provided by

$$\boldsymbol{p}^T(x)=[1, x, y, xy, x^2, y^2, x^2y, xy^2, x^2y^2, \ldots] \tag{6}$$

The coefficients a_i in Eq. (4) can be determined by enforcing Eq. (4) at the n nodes surrounding point x_Q. At node i,

$$u_i=\boldsymbol{p}^T(x_i)\boldsymbol{a} \qquad i=1-n \tag{7}$$

where u_i is the nodal value of u at $x=x_i$. Eq. (7) can be written in the following matrix form:

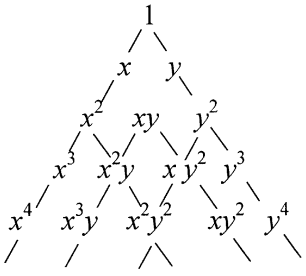

Fig. 1 Pascal's triangle

$$\boldsymbol{u}^e=\boldsymbol{P}_Q\,\boldsymbol{a} \tag{8}$$

where

$$\boldsymbol{U}^e=[\,u_1,\,u_2,\,u_3,\,.....,\,u_n]^T \tag{9}$$

$$\boldsymbol{P}_Q{}^T=[\boldsymbol{p}(x_1),\,\boldsymbol{p}(x_2),\,\boldsymbol{p}(x_3),.....,\,\boldsymbol{p}(x_n)] \tag{10}$$

From Eq. (8),

$$\boldsymbol{a}=\boldsymbol{P}_Q^{-1}\,\boldsymbol{u}^e \tag{11}$$

Hence,

$$u(x)=\,\phi(x)\,\boldsymbol{u}^e \tag{12}$$

where the shape function $\phi(x)$ is defined by

$$\phi(x)=\boldsymbol{p}^T(x)\boldsymbol{P}_Q^{-1}=[\phi_1(x),\,\phi_2(x),\,\phi_3(x),.....,\,\phi_n(x)] \tag{13}$$

The shape function $\phi_i(x)$ obtained through the above procedure satisfies

$$\phi_i\,(x_i)=1 \qquad i=1\sim n \tag{14a}$$

$$\phi_j\,(x_i)=0 \qquad j\neq i \tag{14b}$$

$$\sum_{i=1}^{n}\phi_i(x)=1 \tag{14c}$$

Therefore, the shape functions possess the delta function property, and the essential boundary conditions can be easily imposed in the LPIM.

It is possible that $\boldsymbol{P}_Q^{-1}$ in Eq. (13) does not exist in some situations. This arises, for example, when there are too many nodes in the influence domain sitting on two parallel lines. The above difficulty can be overcome if an appropriate basis is chosen according to the distribution of nodes. Another more generally applicable method is to randomly move nodes by a small distance before computing to avoid the singularity of $\boldsymbol{P}_Q$. This small distance d_{mi} for node i is taken as

$$d_{mi}=\beta\cdot d_i \tag{15}$$

where β is a random coefficient chosen as $-0.2\le\beta\le 0.2$ here. Also, d_i is the shortest distance between node i and its neighbouring nodes. After moving the nodes, the new matrix $\boldsymbol{P}_Q$ is, in general, not singular and $\boldsymbol{P}_Q^{-1}$ can be computed.

A circle of radius r can be used as the influence domain for a point x_Q. The radius r can be obtained according to the node density around the point x_Q. The number of nodes n can be determined by counting all the points in the influence domain. In this paper, the range n=9~25 is used.

4. The local weak form of LPIM

Due to the point interpolation approximation, the essential boundary conditions in Eq. (3) can be imposed directly as in the traditional FEM. A generalized local weak form of the differential Eq. (1), over a local sub-domain Ω_s bounded by Γ_s, can be obtained using the weighted residual method

$$\int_{\Omega_s} w_i(\sigma_{ij,j} + b_i)d\Omega=0 \tag{16}$$

where w_i is the weight function.

The first term on the left hand side of Eq. (16) can be integrated by parts to become

$$\int_{\Gamma_s} w_i\sigma_{ij}n_j d\Gamma-\int_{\Omega_s} (w_{i,j}\sigma_{ij} - w_i b_i)d\Omega=0 \tag{17}$$

The support sub-domain Ω_s of a node x_i is a domain in which $w_i(x)\neq 0$. An arbitrary shaped support domain can be used (see Fig. 2). A circle or rectangular support domain is used in this paper for convenience. It can be found that the boundary Γ_s for the support domain is usually composed of three parts: the internal boundary Γ_{si}, the boundaries Γ_{su} and Γ_{st}, over which the essential and natural boundary conditions are specified. Imposing the natural boundary condition and noticing that $\sigma_{ij}n_j=(\partial u/\partial n) \equiv t_i$ in Eq. (17), it is obtained that

$$\int_{\Gamma_{si}} w_i t_i d\Gamma+ \int_{\Gamma_{su}} w_i t_i d\Gamma+ \int_{\Gamma_{st}} w_i \bar{t}_i d\Gamma- \int_{\Omega_s} (w_{i,j}\sigma_{ij} - w_i b_i)d\Omega=0 \tag{18}$$

For a support domain located entirely within the global domain, there is no intersection between Γ_s and the global boundary Γ, $\Gamma_{si}=\Gamma_s$, and the integrals over Γ_{su} and Γ_{st} vanish.

With Eq. (18) for any node x_i, instead of dealing with a global boundary value problem, the problem becomes a localized boundary value problem over a support domain. In the present formulation, the equilibrium equation and boundary conditions are satisfied in all local support domains Ω_s and on their boundary Γ_s. Although the support domains affect the solution, as long as the union of all the local domains covers the global domain Ω, the equilibrium equation and the boundary conditions will theoretically be satisfied in the global domain Ω and in its boundary Γ (Atluri and Zhu 1998).

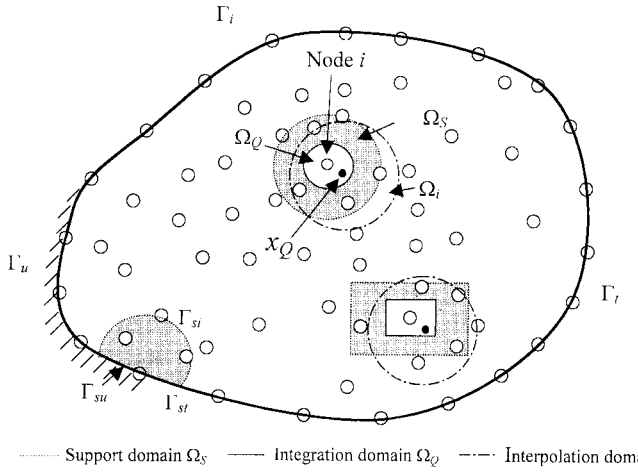

Fig. 2 Support domain Ω_S and integration domain Ω_Q for node i, and the interpolation domain Ω_i for Gauss integration point x_Q

5. Discretization and numerical implementation for the LPIM

5.1 Discrete equations of LPIM

The problem domain Ω is represented by properly scattered nodes. The point interpolation approximation (12) is used to approximate the value of a point x_Q. Substituting Eq. (12) into the local weak form (18) for all nodes leads to the following discrete system of equations:

$$\boldsymbol{K}\boldsymbol{u}_e=\boldsymbol{f} \tag{19}$$

where the "stiffness" matrix $\boldsymbol{K}$ and nodal "load" $\boldsymbol{f}$ vector are defined by

$$\boldsymbol{K}_{ij}=\int_{\Omega_s}\boldsymbol{v}_i^T\boldsymbol{D}\boldsymbol{B}_j d\Omega-\int_{\Gamma_{si}}\boldsymbol{w}_i\boldsymbol{N}\boldsymbol{D}\boldsymbol{B}_j d\Gamma-\int_{\Gamma_{su}}\boldsymbol{w}_i\boldsymbol{N}\boldsymbol{D}\boldsymbol{B}_j d\Gamma \tag{20a}$$

$$\boldsymbol{f}_i=\int_{\Gamma_{st}} w_i\bar{t}_i\, d\Gamma+\int_{\Omega_s}\boldsymbol{w}_i\boldsymbol{b}_i d\Omega \tag{20b}$$

with $\boldsymbol{w}$ being the value of the weight function matrix, corresponding to node i, evaluated at the point x, and

$$\boldsymbol{N}=\begin{bmatrix} n_x & 0 & n_y \\ 0 & n_y & n_x \end{bmatrix} \tag{20c}$$

$$\boldsymbol{B}_j=\begin{bmatrix} \phi_{j,x} & 0 \\ 0 & \phi_{j,y} \\ \phi_{j,y} & \phi_{j,x} \end{bmatrix} \tag{20d}$$

$$\boldsymbol{v}_i=\begin{bmatrix} w_{i,x} & 0 \\ 0 & w_{i,y} \\ w_{i,y} & w_{i,x} \end{bmatrix} \tag{20e}$$

$$\boldsymbol{D}=\begin{bmatrix} 1 & \upsilon & 0 \\ \upsilon & 1 & 0 \\ 0 & 0 & (1-\upsilon)/2 \end{bmatrix} \quad \text{for plane stress} \tag{20f}$$

It can be easily seen that the system stiffness matrix $\boldsymbol{K}$ in the present method is banded but asymmetric.

5.2 Weight function

As the LPIM is regarded as a weighted residual method, the weight function plays an important role in the performance of the method. Theoretically, as long as the condition of continuity is satisfied, any weight function is acceptable. However, the local weak form is based on the local sub-domains of all the nodes in the problem domain. It can be shown that weight functions which decrease in magnitude with increasing distance from the point x_Q to the node x_i yields better results. Therefore, weight functions which only depend on the distance between the two points are considered here. Both parabolic and spline weight functions are used.

Weight function A: the 2-order parabolic function

$$w_i(x)=\begin{cases} 1-\left(\dfrac{d_i}{r_w}\right)^2 & 0 \le d_i \le r_w \\ 0 & d_i \ge r_i \end{cases} \tag{21a}$$

Weight function B: the spline function

$$w_i(x)=\begin{cases} 1-6\left(\dfrac{d_i}{r_w}\right)^2+8\left(\dfrac{d_i}{r_w}\right)^3-3\left(\dfrac{d_i}{r_w}\right)^4 & 0 \le d_i \le r_w \\ 0 & d_i \ge r_w \end{cases} \tag{21b}$$

where $d_i=|x_Q-x_i|$ is the distance from node x_i to point x_Q, and r_w is the size of the support for the weight function.

5.3. Numerical integration

Numerical integration is needed to evaluate the integrals in Eqs. (20a) and (20b). Gauss quadrature is used in the LPIM. For a node x_i, a local integration cell is needed to employ Gauss quadrature. For each Gauss quadrature point x_Q, point interpolation is performed to obtain the integrand. Therefore, for a node x_i, there exist three local domains: local integration domain Ω_Q (size r_q), weight function domain Ω_w (same as Ω_s) for $w_i\neq 0$ (size r_w), and interpolation domain Ω_i for x_Q (size r_i). These three local domains are independent as long as the condition $r_q \le r_w$ is satisfied. It should be noted that the weight function w is zero along the boundary of the integration domain if the integration and weight domains are the same ($r_q=r_w$). Hence, Eq. (20b) can be simplified because the integration along the internal boundary Γ_{si} vanishes.

There exist difficulties in obtaining exact numerical integration in meshless methods (Atluri *et al*. 1999, Dolbow and Belytschko 1999, and Liu and Yan 1999). Insufficiently accurate numerical integration may cause a deterioration and a rank-deficiency in the numerical solution. The numerical integration errors result from the complexity of the integrand. First, the shape functions constructed using the point interpolation approximation have a complex feature. The shape functions have different forms in each small integration region. The derivatives of the shape functions may have oscillations. Second, the overlapping of interpolation domains makes the integrand in the overlapping domain very complicated. In order to guarantee the accuracy of the numerical integration, Ω_Q should be divided into some regular small partitions. In each small partition, more Gauss quadrature points should be used.

5.4 Imposition of essential boundary conditions

In the MLPG method, it is difficult to implement essential boundary conditions because the shape functions constructed by the MLS approximation lack the delta function property. Strategies have been developed for alleviating the above problem, such as using the Lagrange multiplier method, the penalty method, and the direct interpolation method. In the LPIM, because the shape functions possess the delta function property, the essential boundary conditions can be implemented with ease. Since the system equations of the LPIM are assembled based on nodes as in the finite difference

method, the items of the row in the matrix $\boldsymbol{K}$ for the nodes on the essential boundary need not even be computed. This reduces the computational cost, especially when the number of nodes on the essential boundary is large.

6. Numerical examples

The LPIM is coded in FORTRAN. Cases are run in order to examine the LPIM in two-dimensional elastostatics. Because the problem domains in the examples are rectangles, rectangular sub-domains are used for establishing the weight function. The size of the sub-domain for node i is defined as

$$d_s=\alpha\, d_i \tag{22}$$

where α is a coefficient which lies in the range 0.5-3.0 in this paper, and d_i is the shortest distance between node i and its neighbouring nodes.

6.1 Standard patch test

The first numerical example is the standard patch test. The two patches shown in Fig. 3 are tested. Fig. 3(a) shows a patch with 9 nodes of which one is an interior node. Fig. 3(b) shows a patch of 25 nodes including 9 irregularly-placed interior nodes.

In these patch tests, the displacements are prescribed on all outside boundaries by a linear function of x and y on the patches of dimensions L_x=2.0 by L_y=2.0. The parameters are taken as E=1.0 and ν=0.3. The linear displacement functions are u_x=0.6x and u_y=0.6y. Satisfaction of the patch test requires that the displacement of any interior node be given by the same linear functions and that the strains and stresses be constant in the patch.

Six to nine nodes are used in the interpolation for a point x_Q depend on the distances between the

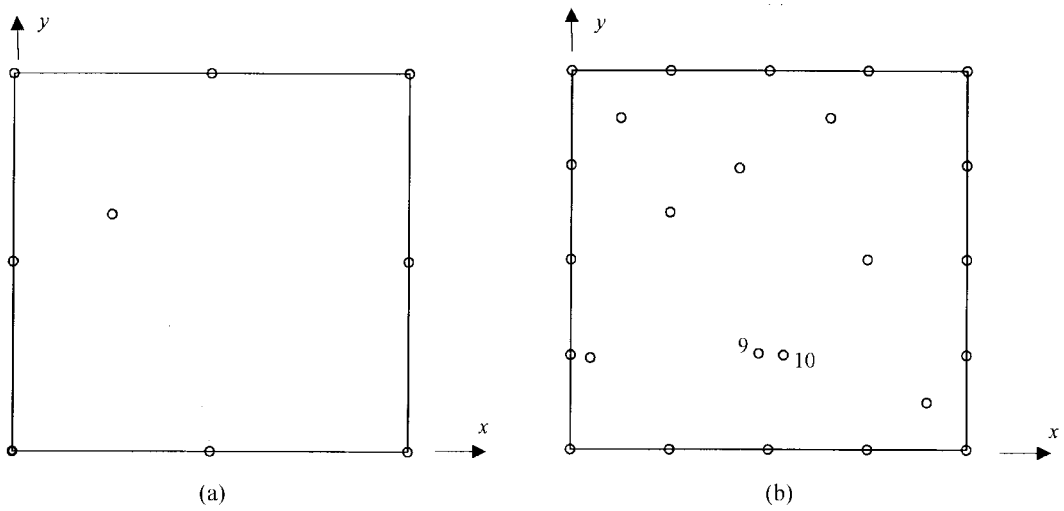

Fig. 3 9-node and 25-node patches

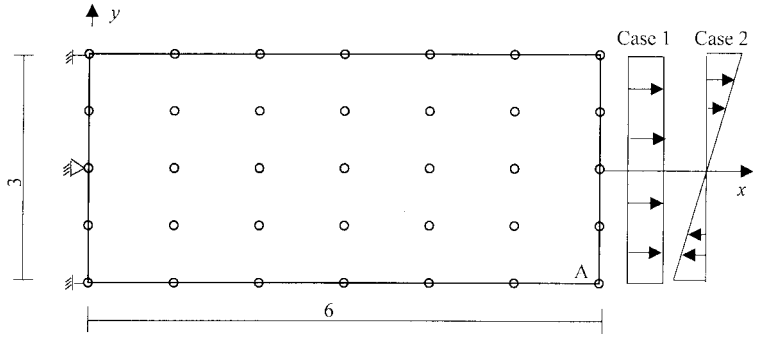

Fig. 4 Nodes on a higher-order patch

nodes and the point x_Q. The computational results show that the LPIM passes the patch test exactly. In Fig. 3(b), nodes 9 and 10 are deliberately placed close to each other. It is found that this does not affect the computational results.

6.2 Higher-order patch test

The higher-order patches shown in Fig. 4 are used to study the effect of the weight functions and the size of the support domain. In case 1, a uniform axial stress of unit intensity is applied on the right end. The exact solution for this problem with E=1 and v=0.25 is: $u_x=x$ and $u_y=-y/4$. In case 2, a linearly varying normal stress is applied on the right end. The exact solution for this problem with E=1 and v=0.25 is: $u_x=2xy/3$ and $u_y=-(x^2+y^2/4)/3$. Nine nodes are used in the interpolation. It can be found that case 1 is passed exactly using both the parabolic and spline weight functions. The computational results for case 2 are shown in Table 1. It can be found that case 2 is passed exactly using the parabolic weight function for all support domain sizes. When the spline weight function is used, case 2 is passed exactly for small support domains. If the size of the support domain is large, the test fails.

The reason for the failure is the numerical integration errors of the complex integrands. The parabolic weight function is simpler than the spline weight function. Hence, exact numerical integration can be achieved more easily using the parabolic weight function. In order to study the effect of numerical integration, several cases with different Gauss quadrature points and sub-divisions for integration are computed. The results are shown in Table 1. It can be found that the accuracy of the solution improves with the improvement of the numerical integration. However, since the continuity order of the spline weight function is higher than that of the 2-order parabolic

Table 1 Relative errors (%) at point A for higher-order patch test case 2 (n_d, number of sub-division; n_g, Gauss points in each sub-division)

	α=1.0			α=1.5			α=2.0		
	n_d=1, n_g=4	n_d=1, n_g=10	n_d=2×2, n_g=4	n_d=1, n_g=4	n_d=1, n_g=10	n_d=2×2, n_g=4	n_d=1, n_g=4	n_d=1, n_g=10	n_d=2×2, n_g=4
Function A	0.0	0.0	0.0	0.0	0.0	0.0	0.0	0.0	0.0
Function B	0.0	0.0	0.0	0.83	3.3×10^{-3}	2×10^{-4}	1.1	1×10^{-2}	6×10^{-4}

weight function, the spline weight function can yield better results for many practical problems with high gradients of stresses.

6.3 Cantilever beam

The cantilever beam shown in Fig. 5 is considered. The beam is of length L and height D subjected to a parabolic traction at the free end. The beam has a unit thickness and a plane stress problem is considered. The analytical solution is available and can be found in Timoshenko and Goodier (1970). The displacements are given by

$$u_x=-\frac{Py}{6EI}\left[(6L-3x)x+(2+\nu)\left(y^2-\frac{D^2}{4}\right)\right] \tag{23a}$$

$$u_y=-\frac{Py}{6EI}\left[3\nu y^2(L-x)+(4+5\nu)\frac{D^2x}{4}+(3L-x)x^2\right] \tag{23b}$$

and the stress components are

$$\sigma_x(x,y)=-\frac{P(L-x)y}{I} \tag{24a}$$

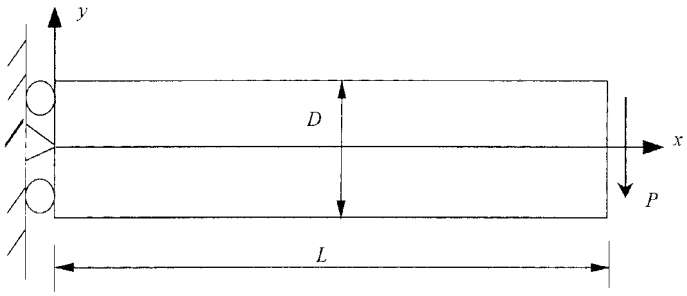

Fig. 5 Cantilever beam

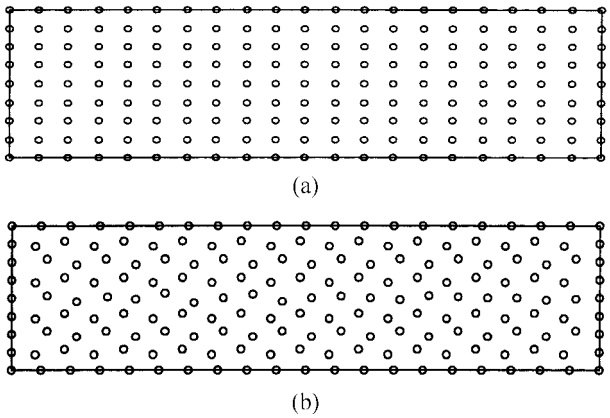

Fig. 6 (a) Regular distribution of nodes for cantilever beam, (b) Irregular distribution of nodes for cantilever beam

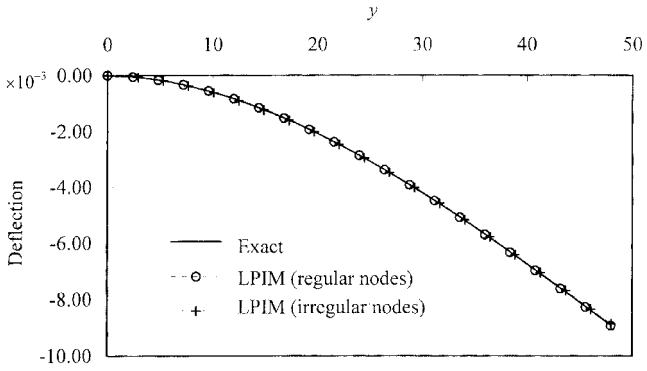

Fig. 7 Deflection of beam

$$\sigma_y(x,y)=0 \tag{24b}$$

$$\tau_{xy}(x,y)=\frac{P}{2I}\left[\frac{D^2}{4}-y^2\right] \tag{24c}$$

The parameters are taken as E=3.0×10^7, ν = 0.3, D =12, L = 48, and P =1000. Both regular and irregular distributions of nodes as shown in Fig. 6 are employed.

Fig. 7 shows a comparison of the analytical solution and the present numerical solution for the beam deflection along the x-axis. The plot shows excellent agreement between the analytical and numerical results. Fig. 8 illustrates the comparison between the shear stress at the section x=L/2 calculated analytically and using the LPIM. Again, very good agreement is observed for both regular and irregular distributions of nodes.

For the error analysis, the energy norm is defined as the error indicator, as the accuracy in strain or stress is much more critical than the displacements.

$$e_e=\left\{\int_\Omega \left(\varepsilon^{LPIM}-\varepsilon^{EXACT}\right)^T D\left(\varepsilon^{LPIM}-\varepsilon^{EXACT}\right)d\Omega\right\}^{1/2} \tag{25}$$

The convergence of LPIM is studied. The regular distribution of nodes is used for comparison. The

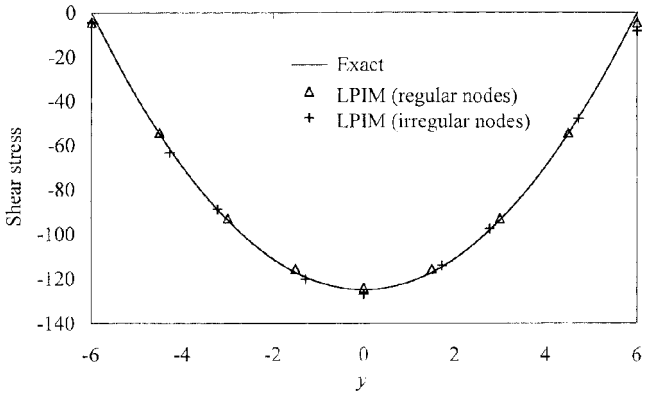

Fig. 8 Shear stress σ_{xy} at section x=L/2 of beam

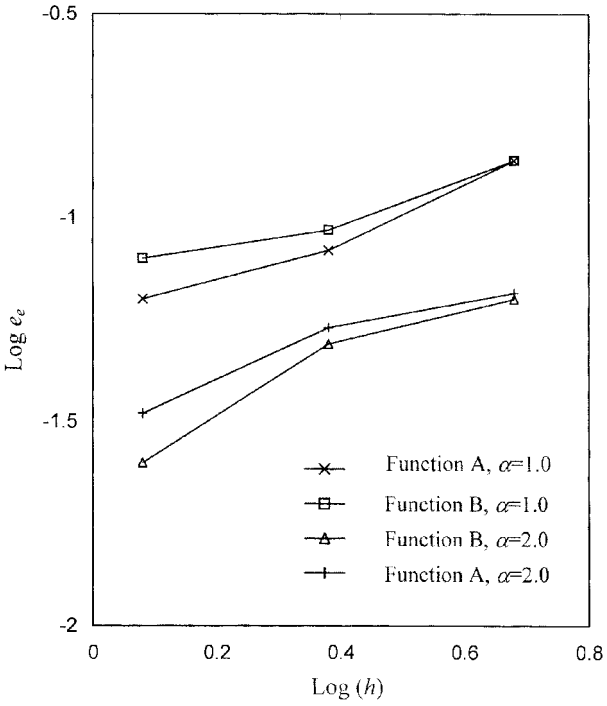

Fig. 9 Convergence in norm of error e_e

investigation is done for α=1.0 and 2.0 using both the 2-order parabolic weight function and the spline weight function. The convergence with mesh refinement is shown in Fig. 9. Here, h is equivalent to the maximum element size in the FEM analysis. It is observed that the convergence of LPIM is very good. Comparing the results obtained using different sub-domain sizes, it can be found that a bigger-sized sub-domain gives better accuracy provided that the numerical integration is accurate. From Fig. 9, it is found that using the parabolic weight function produces better results than using the spline weight function. As discussed above, the reason is that the parabolic weight function is easer for obtaining exact numerical integration than the spline weight function.

6.4 Hole in an infinite plate

Consider now a plate with a central circular hole: $x^2+y^2 \le a^2$, subjected to a unidirectional tensile load of 1.0 in the x-direction as shown in Fig. 10. Due to symmetry, only the upper right quadrant of the plate is modeled. Plane strain conditions are assumed, and the material constants are E=1.0×10^3, and ν=0.3. Symmetry conditions are imposed on the left and bottom edges, and the inner boundary of the hole is traction free. The exact solution for the stresses in an infinite plate with a central circular hole is

$$\sigma_x(x,y)=1-\frac{a^2}{r^2}\left\{\frac{3}{2}\cos 2\theta+\cos 4\theta\right\}+\frac{3a^4}{2r^4}\cos 4\theta \tag{26a}$$

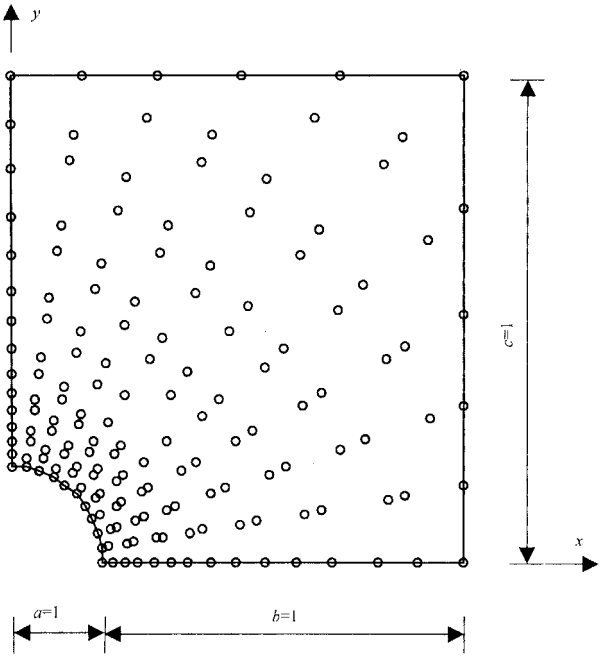

Fig. 10 Nodes on plate with central hole subjected to unidirectional tensile load in *x*-direction

$$\sigma_y(x,y)=-\frac{a^2}{r^2}\left\{\frac{1}{2}\cos 2\theta-\cos 4\theta\right\}-\frac{3a^4}{2r^4}\cos 4\theta \tag{26b}$$

$$\sigma_{xy}(x,y)=-\frac{a^2}{r^2}\left\{\frac{1}{2}\sin 2\theta+\sin 4\theta\right\}+\frac{3a^4}{2r^4}\sin 4\theta \tag{26c}$$

where (r, θ) are the polar coordinates and θ is measured counter-clockwise from the positive x axis. Traction boundary conditions given by the exact solution (26) are imposed on the right (x=5) and top (y = 5) edges.

The results are obtained using two kinds of nodal arrangements: 54 nodes and 165 nodes. The nodal arrangement of 165 nodes is shown in Fig. 10. It is found that the results for the displacements are identical. As the stresses are more critical, detailed results are presented here. The stress σ_{xx} at x =0 obtained using the LPIM is shown in Fig. 11. It can be observed from Fig. 11 that the LPIM yields satisfactory results for the problem considered. The convergence of the present method is also demonstrated in this figure. As the number of nodes increases, the results obtained approaches the analytical solution.

6.5 Stress distribution in a dam

The proposed LPIM is applied to the stress analysis of a dam subjected to hydrostatic pressure on both sides of the dam, as shown in Fig. 12. The problem is solved for the plane strain case with E=30 Gpa and v=0.15. The nodal arrangement is shown in Fig. 13. The problem is also analyzed using the FEM software, ABAQUS.

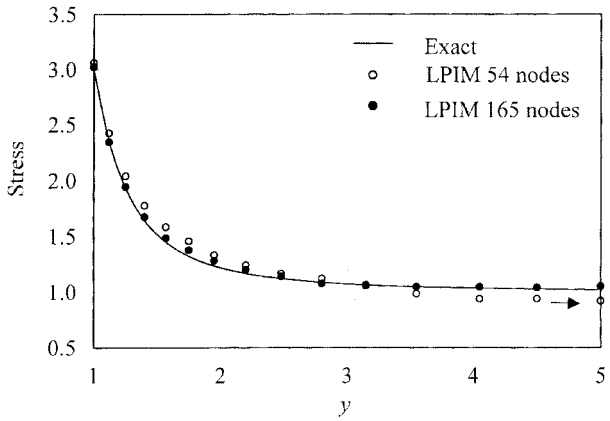

Fig. 11 Stress distribution in plate with central hole subjected to unidirectional tensile load (σ_{xx} at x=0)

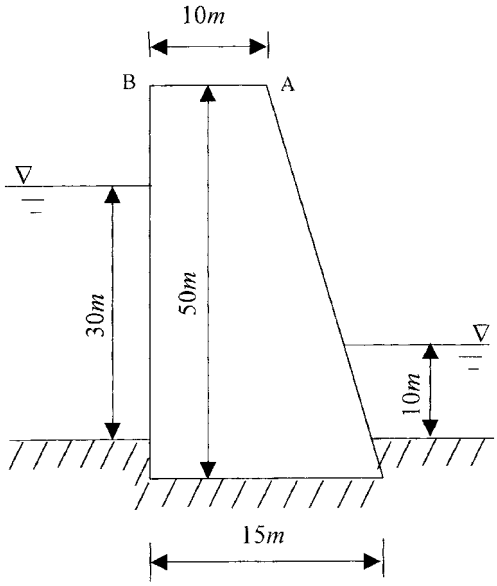

Fig. 12 Dam subjected to hydrostatic pressure

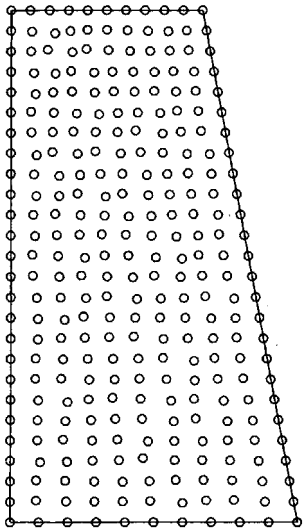

Fig. 13 Arrangement of nodes on dam

The displacements at two corner nodes A and B are listed in Table 2. The results obtained by the present LPIM are in very good agreement with those obtained using the FEM. The distribution of the stress σ_{yy} in the domain obtained by FEM and PIM are shown in Fig. 14. It is seen that the

Table 2 Displacements ($\times 10^{-3}$) at points A and B of the dam

Nodes	x	y	LPIM		FEM	
			u_x	u_y	u_x	u_y
A	10.0	50.0	2.468	−0.142	2.445	−0.140
B	0.0	50.0	2.468	0.382	2.445	0.376

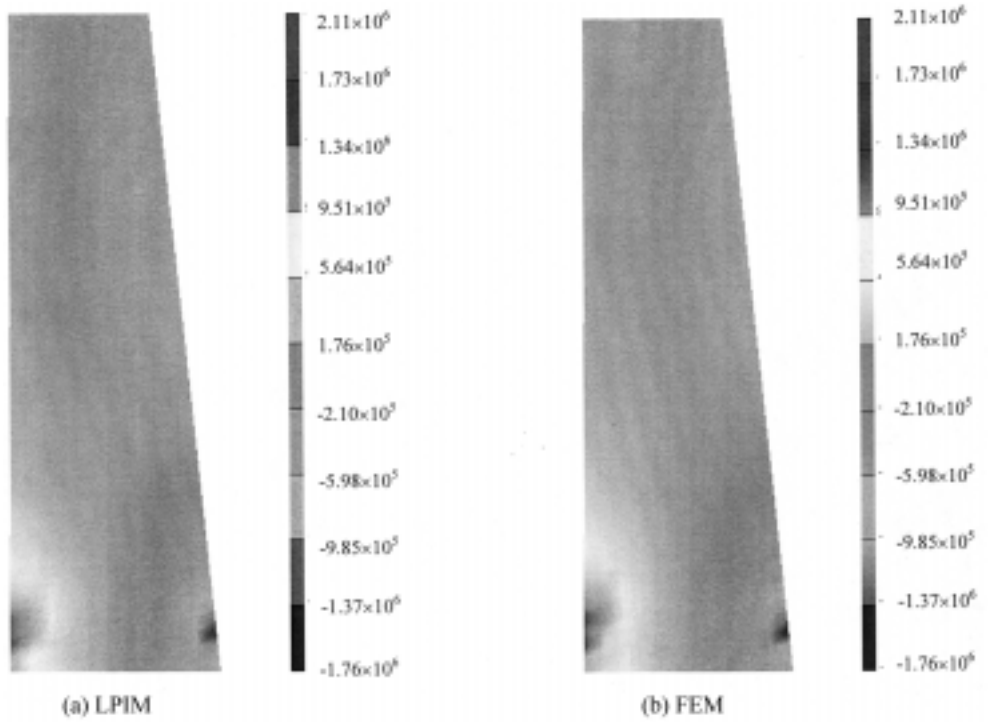

Fig. 14 Distribution of stress σ_{yy}

LPIM gives satisfactory results for this problem.

7. Discussion and conclusions

A local point interpolation method (LPIM) has been presented. In the LPIM, a technique is proposed to construct polynomial interpolation functions with the delta function property using a group of arbitrarily distributed points. A local weak form, based on the point interpolation approximation, is developed using the weighted residual method for two-dimensional solids. Numerical examples have demonstrated the effectiveness for elastostatics of the present LPIM. Compared to other meshless methods, the present LPIM is an improvement for the following reasons:

(a) The LPIM is a truly meshless method based on non-element interpolation and non-mesh integration.

(b) The imposition of essential boundary conditions is easy in LPIM due to the delta property of the shape functions.

(c) The computational cost is much lower because of the simple interpolation and the reduction in the computation of the stiffness matrix.

The present method is very easy to implement, and very flexible for calculating displacements and stresses of desired accuracy in solids. As a truly meshless method, the present LPIM opens an alternative avenue to develop adaptive analysis codes for stress analysis in solids and structures.

References

Atluri, S.N., Kim, H.G. and Cho J.Y. (1999), "A critical assessment of the truly meshless local Petrov-Galerkin (MLPG), and local boundary integral equation (LBIE) methods", *Computational Mechanics*, **24**, 348-372.

Atluri, S.N. and Zhu, T. (1998), "A new meshless local Petrov-Galerkin (MLPG) approach in computational mechanics", *Computational Mechanics*, **22**, 117-127.

Atluri, S.N. and Zhu, T. (2000), "New concepts in meshless methods", *Computational Mechanics*, **22**, 117-127.

Belytschko, T., Lu, Y.Y. and Gu, L. (1994), "Element-free Galerkin methods", *Int. J. Numer. Methods Engrg.*, **37**, 229-256.

Belytschko, T. and Organ, D. (1995), "Coupled finite element−element−free Galerkin method", *Computational Mechanics*, **17**, 186-195.

Dolbow, J. and Belytschko, T. (1999), "Numerical itegration of the Galerkin weak form in meshfree methods", *Computational Mechanics*, **23**, 219-230.

Gu, Y.T. and Liu, G.R. (2000a), "A coupled element free Galerkin/boundary element method for stress analysis of two-dimensional solids", *Computer Methods Appl. Mech. Engrg* (in press).

Gu, Y.T. and Liu, G.R. (2000b), "A boundary point interpolation method for stress analysis of solids", *Computational Mechanics* (in press).

Hegen, D. (1996), "Element-free Galerkin methods in combination with finite element approaches", *Computer. Methods Appl. Mech. Engrg*., **135**, 143-166.

Kothnur, V.S., Mukherjee, S. and Mukherjee, Y.X. (1999), "Two-dimensional linear elasticity by the boundary node method", *Int. J. Solids Structures*, **36**, 1129-1147.

Liu, G.R. (1999), "A point assembly method for stress analysis of solids", *Impact Response of Materials and Structures*, Ed. by Shim, V.P.W., Oxford, 475-480.

Liu, G.R. and Gu, Y.T. (1999), "A point interpolation method", *Proceedings of the Fourth Asia-Pacific Conference on Computational Mechanics*, Singapore, 1009-1014.

Liu, G.R. and Gu, Y.T. (2000a), "Coupling element free Galerkin and hybrid boundary element methods using modified variational formulation", *Computational Mechanics*, **26**, 166-173.

Liu, G.R. and Gu, Y.T. (2000b), "Coupling of element free Galerkin method with boundary point interpolation method", *Proceedings of Advances in Computational Engineering and Science*, Los Angeles, 1427-1432.

Liu, G.R. and Yan, L. (1999), "A study on numerical integration in element free methods", *Proceedings of the Fourth Asia-Pacific Conference on Computational Mechanics*, Singapore, 979-984.

Liu, G.R. and Yan, L. (2000), "A modified meshless local Petrov-Galerkin method for solids mechanics", *Proceedings of Advances in Computational Engineering and Science*, Los Angeles, 1374-1379.

Liu, G.R. Yang, K.Y. and Wang, J.G. (2000), "A constraint moving least squares method in meshless methods", (submitted).

Liu, W.K., Jun, S. and Zhang, Y.F. (1995), "Reproducing kernel particle methods", *Int. J. Numer. Methods Engrg*., **20**, 1081-1106.

Nayroles, B., Touzot, G. and Villon, P. (1992), "Generalizing the finite element method: diffuse approximation and diffuse elements", *Computational Mechanics*, **10**, 307-318.

Timoshenko, S.P. and Goodier, J.N. (1970), *Theory of Elasticity*, 3rd Ed., McGraw-Hill, New York.